Building A Portable Room Temperature Quantum Memory

A Thesis presented

by

Ruoxi Wang

to

The Graduate School

in Partial Fulfillment of the

Requirements

for the Degree of

Master of Arts

in

Physics

Stony Brook University

August 2016

Stony Brook University

The Graduate School

Ruoxi Wang

We, the thesis committe for the above candidate for the

Master of Arts degree, hereby recommend

acceptance of this thesis

Eden Figueroa - Thesis Advisor
Associate Professor of Department of Physics and Astronomy

Xu Du - Second Reader
Associate Professor of Department of Physics and Astronomy

Jacobus Verbaarschot
Professor of Department of Physics and Astronomy

This thesis is accepted by the Graduate School

Charles Taber
Dean of the Graduate School

Abstract of the Thesis

Building A Portable Room Temperature Quantum Memory

by

Ruoxi Wang

Master of Arts

in

Physics

Stony Brook University

2016

Quantum memory provides a platform for building quantum networks in quantum information processing. Applications of said networks include quantum gates for quantum computing and quantum repeaters for long distance quantum key distribution. An optical quantum memory can be realized by a cold atom system combined with electromagnetically induced transparency (EIT). However, room temperature quantum memory via vapor cells benefit from its easy operation without the need for laser cooling and trapping, promoting the scalability. In this work, we studied and tested EIT in a Rubidium vapor cell at room temperature, by storing and retrieving a classical light source using probe and control lasers. We also constructed a portable quantum memory system and realized the storage of light at the single-photon level at room temperature. For a future perspective, we designed the quantum memory system with cavities, wishing to breakthrough in storage efficiency.

Contents

List of Figures

List of Tables

Acknowledgements

Thanks Professor Eden Figueroa and everyone in his lab, especially Mehdi Namazi for helping me with this thesis. Thanks Connor Goham, Marty Cohen, Bertus Jordaan, Steven Sagona, Sonali Gera, Reihaneh Shahrokhshahi for kind help.

All the best!

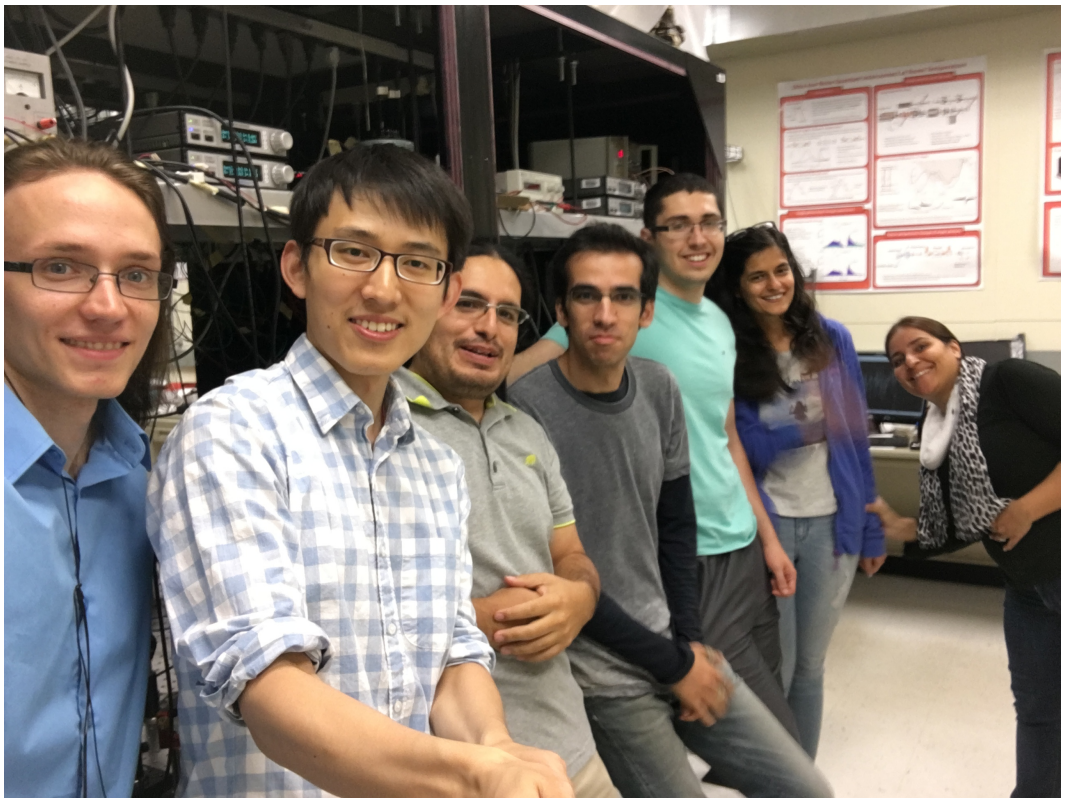

Chapter 1

Introduction

The capability of classical computers has exponentially improved as the size of processors shrank and became more dense every year since the dawn of transistors, which is known as the familiar "Moore's Law"[1]. Unfortunately, the days that "Moore's Law" can remain accurate are limited as the chip holding the silicon can only continue to shrink until it reaches the molecular and atomic level, which is ruled by quantum mechanics. Even though splitting the atom will not improve the computing power of computers, there is much more we can do taking advantage of quantum mechanics as Richard Feynman has foreseen, detailed in his lecture "There's Plenty of Room at the Bottom". [2, 3]

The room is hidden in the quantum bit or "qubit". By taking advantage of the superposition and entanglement of quantum systems, qubits would potentially make breakthroughs for computers where "Moore's Law" is slowing. A qubit can be prepared by the superposition of orthogonal quantum states. Examples include: up and down spin, horizontal and vertical polarization, light with different photon number (known as "Fock state"), etc[4]. For a two-level system:

$$|\psi\rangle = \alpha\,|0\rangle + \beta\,|1\rangle \tag{1.1}$$

where $|\alpha|^2$ and $|\beta|^2$ are the probabilities of measuring the corresponding state. For N qubits with entanglement:

$$|\psi\rangle = \alpha_0\,|0_1 0_2 0_3 ... 0_N\rangle + \alpha_1\,|0_1 0_2 0_3 ... 1_N\rangle + ... + \alpha_0\,|1_1 1_2 1_3 ... 1_N\rangle \tag{1.2}$$

In a classical system, we need N independent capacitors to process information of N digits, whereas in an N-qubit quantum system, the information can be stored in 2^N digits and calculated with parallelism. The potential power of quantum computing can be seen through quantum algorithms which can complete a calculation that would take exponentially longer by a classical computer. One famous example is Shor's algorithm for factoring large numbers [5]), based on which many classically encrypted codes can be possibly deciphered but, unfortunately, not in a limited, reasonable time by classic computing. Nevertheless, what quantum information brings to us is far more benefit than disastrous.

By sharing entangled photon qubits, Alice could teleport the information to Bob from far distance through Bell measurement, known as quantum teleportation [6, 7] The entangled qubits can be recreated by parametric down-conversion (PDC) of nonlinear crystal[8], based on which, the cryptography key distribution can be used to securely protect the information through quantum mechanics[9].

The theoretical protocols in quantum information have been well developed based on quantum theory however, there is a long way to go for experimental realization of scalable quantum information. Photons and atoms are good candidates and commonly used for quantum information processing[3]. Atoms can be laser controlled and trapped to be initialized which allows them to be kept in superposition with high stability. By storing qubits in electronic states of atoms and mapping them onto the collective motion of atoms, trapped atomic ions are well-suited for large-scale quantum computing[10, 11]. Quantum optics is crucial for quantum information technology because of the ability of photons to enable long distance communication and interaction with atoms.

Because of the limited efficiency of the information transferring over the long distance or noisy channels, the signal requires amplifier to copy and amplify the signal. However the direct amplification is not possible for quantum communication due to the no-cloning theorem of quantum mechanics[12]. Taking the advantage of quantum mechanics itself, this problem can be solved by quantum repeater based on the entanglement swapping to amplify the entangled pair for long distance transmission[13–15]. The scheme is shown in Figure 1.1.

In order to perform the entanglement swapping operation, the state of one created entanglement should be stored until the neighboring entanglement is established, as the same requirement for higher-order entanglement swapping[13]. This thus requires "quantum memory" that is able to store a quantum state for a relatively long time and retrieve the state later[16, 17].

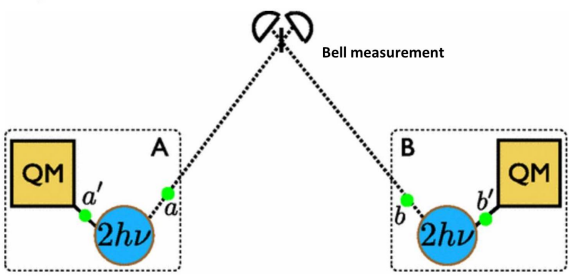

(A) Entanglement swapping using Bell measurement

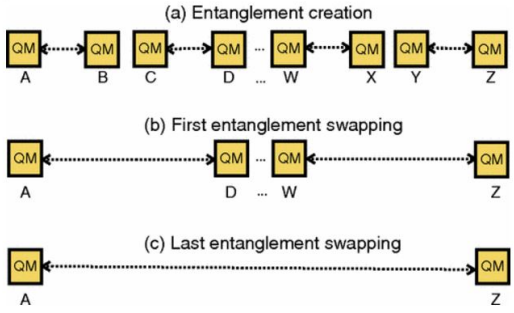

(B) Hierarchical operation of quantum repeaters to distribute entanglement over long distribute between A and Z

FIGURE 1.1: Diagram of quantum repeaters

The essence of quantum memory is the reversible conversion between the qubits of photonic states and atomic states[17]. An ideal quantum memory system should hold the following abilities:

- Able to store qubits in single-photon level
- Capable of cascadability
- Store with good efficiency and high fidelity.
- Preserve the entanglement
- Easily operated and economically accessible for scalable production

The storage of a quantum state can realized using a quantum electrodynamics (QED) system by mapping photon states onto either collective states of atoms or single-atom based on the electromagnetically induced transparency(EIT) techniques[17–19]. These systems always requires laser-cooling and trapping atoms to initialize them to stable quantum state.

An alternate approach is to construct the quantum memories at room temperature with atomic vapors holding the energy structure for EIT schemes[20, 21]. A probe field can interact with isotopic Rubidium vapor atoms in the presence of a control field through EIT and stored in the atomic states. The efficiency of the storage corresponds to the storage time when the control field is off. The easy-to-operate room temperature memory system also has the advantage in building a portable quantum memory platform such that it is flexible for further scalable quantum information process. By adding the cavity to the EIT system to strengthen the light-matter interaction, the storage efficiency could greatly improve. To realized the quantum memory, the polarization of light should be encoded to the single photon as a qubit, stored, and recreated with the high fidelity. The details about the above are described in the following chapters of this thesis.

Chapter 2

Electromagnetically induced transparency

The development of Electromagnetically Induced Transparency (EIT) has allowed for strong advances in the field of quantum information technology. In particular it has been shown to be useful for the slowdown and storage of light which is critical for some quantum logic gate applications as well as quantum communication[17, 22]. For example, for long distance quantum communication, decoherence of the transmitted photon limits how far a qubit can be sent.[13] Quantum repeaters built upon quantum memories in which photon qubits can be preserved and stored are a promising solution to this issue, and EIT is a good candidate method to make this possible.

With room temperature quantum memory, EIT allows us to use a control optical field to make an atomic vapor transparent around an atomic resonance. We can then propagate a weak probe field (even a single photon) through the medium without absorption. The effect of EIT is that the group velocity of the light that the medium is now transparent to can be significantly reduced. This effectively compresses the light pulse in space and if made slow enough it can be stored in the medium.

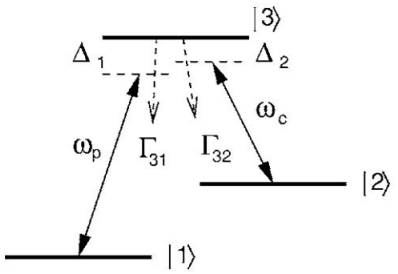

FIGURE 2.1: EIT Lambda system: Λ system with a ground state $|1\rangle$, a metastable state $|2\rangle$, and excited state $|3\rangle$. The probe field has frequency ω_p and the control field has frequency ω_c. The probe laser has detuning $\Delta_1 = \omega_{31} - \omega_p$ and the control laser addresses the has detuning $\Delta_2 = \omega_{32} - \omega_c$ from atomic resonances. Γ_{ik} denote the decay rate from $|i\rangle$ to $|k\rangle$. $|1\rangle$ and $|2\rangle$ are dipole-forbidden resulting in an negligible decay rate.

In an three-level atomic system, the weak probe light drives the atoms into a superposition of the Zeeman sublevels. This coupling between light and atoms via this Raman transition is known as a dark state polariton.

By adiabatically ramping down the coherent field Rabi frequency one can smoothly transfer the light state into the atomic Zeeman sublevels for storage. After waiting a variable storage time the coherent light can then be ramped back up and the qubits can be imprinted back onto a photon and released[17].

2.1 EIT theory

2.1.1 Dark states

EIT can be seen as the result of the interference of between different excitation pathways resulting in a "dark state"[23]. In a three-level atomic system as is shown in Figure 2.1, a probe field with frequency ω_p driving $|1\rangle$- $|3\rangle$ transition is coherently coupled to a strong control field with ω_c driving$|2\rangle$-$|3\rangle$ transition. The excited state $|3\rangle$ is thus driven mainly by pathway: $|1\rangle$-$|3\rangle$ or indirect $|1\rangle$-$|3\rangle$-$|2\rangle$-$|3\rangle$. The latter one has low probability due to the limited decay rate to state $|2\rangle$. There also exist higher order pathways with negligible amplitude. Under strong control field, the first two pathways would has equal magnitude and destructive interference to cause no absorption of photons thus a transparency window occurs.

The atom-laser interaction Hamiltonian for a EIT system can be written in approximation in terms of Rabi frequency $\Omega = \mathbf{d} \cdot \mathbf{E}/\hbar$ where $\mathbf{E}$ is the electric field and $\mathbf{d}$ is the transition electronic dipole moment. For the three-atom system, the Hamiltonian is

$$H_{int} = -\frac{\hbar}{2}\begin{bmatrix} 0 & 0 & \Omega_p \\ 0 & -2(\Delta_1 - \Delta_2) & \Omega_c \\ \Omega_p & \Omega_c & -2\Delta_1 \end{bmatrix} \tag{2.1}$$

Here $\Delta_1 = \omega_{31} - \omega_p$ is the probe field detuning from $|1\rangle \rightarrow |3\rangle$ transition and $\Delta_2 = \omega_{32} - \omega_c$ is the coupling field detuning from $|2\rangle \rightarrow |3\rangle$ transition. The single-photon detuning is $\Delta = \Delta_1$ and the two-photon detuning is $\delta = \Delta_1 - \Delta_2$. For $\delta = 0, \Delta_2 = \Delta_1 = \Delta$, which is the two-photon resonance, the eigenstates of H_{int} can then be solved and written in basis of the bare atom states:

$$\left|a^+\right\rangle = \sin\theta \sin\phi \left|1\right\rangle + \cos\theta \sin\phi \left|2\right\rangle + \cos\phi \left|3\right\rangle \tag{2.2}$$

$$\left|a^0\right\rangle = \cos\theta \left|1\right\rangle - \sin\theta \left|2\right\rangle \tag{2.3}$$

$$\left|a^-\right\rangle = \sin\theta \cos\phi \left|1\right\rangle + \cos\theta \cos\phi \left|2\right\rangle - \sin\phi \left|3\right\rangle \tag{2.4}$$

where θ and ϕ are defined as $\tan\theta = \Omega_p/\Omega_c$ and $\tan 2\phi = \sqrt{\Omega_p^2 + \Omega_c^2}/\Delta$.

The state $\left|a^0\right\rangle$ is superposition of state $|1\rangle$ and$|2\rangle$ and has no amplitude of state $|3\rangle$. The transition amplitude from $\left|a^0\right\rangle$ to the excited state $|3\rangle$ is

$$T_{a^0->3} = \langle 3| H_{int} \left|a^0\right\rangle = 0 \tag{2.5}$$

This means $\left|a^0\right\rangle$ is the dark state. In the limit of strong coupling field, $\Omega_p \ll \Omega_c$, it reduces to the ground state $\left|a^0\right\rangle = |1\rangle$ with no excitation. Furthermore as the probe is on resonance meaning $\Delta = 0$, the two dressed states become $|a^+\rangle = 1/\sqrt{2}(|2\rangle + |3\rangle)$ and $|a^-\rangle = 1/\sqrt{2}(|2\rangle - |3\rangle)$. The dark

state can be initially prepared in ground state $|1\rangle$ through the optical pumping or to another dark state by adopting adiabatic evolution of the field[23].

2.1.2 Linear susceptibility

The properties of EIT can be predicted by the susceptibilities of the atomic medium. Here we study the linear (first order) susceptibilities, which is defined as

$$\boldsymbol{P} = \epsilon_o \chi^{(1)} \boldsymbol{E} \tag{2.6}$$

The optical properties of the atomic medium are characterized by the linear susceptibility $\chi^{(1)}$ since its imaginary part, Im$[\chi^{(1)}]$, determines the absorption of the field by atoms while the real part, Re $[\chi^{(1)}]$, characterizes the refractive index (dispersion).

The linear susceptibility can be derived through the time-dependent Hamiltonian of the interaction picture governed by the master equation of atomic density operator. The details are described in [23] followed by the result:

$$\chi^{(1)} = \frac{|d_{13}|^2 \varrho}{\epsilon_0 \hbar} \times [\frac{4\delta(|\Omega_c|^2 - 4\delta\Delta) - 4\Delta\gamma_{21}^2}{||\Omega_c|^2 + (\gamma_{31} + 2i\Delta)(\gamma_{21} + 2i\delta)|^2} + i\frac{8\delta^2\gamma_{31} + 2\gamma_{21}(|\Omega_c|^2 + \gamma_{31}\gamma_{21})}{||\Omega_c|^2 + (\gamma_{31} + 2i\Delta)(\gamma_{21} + 2i\delta)|^2}] \tag{2.7}$$

Here $\varrho = N_{atom}/V$ is the density of atoms, γ_{ik} is the coherence decay rate from state $|i\rangle$ to $|k\rangle$. The features of the real and imaginary parts are simulated as a function of the detuning in Figure 2.2.

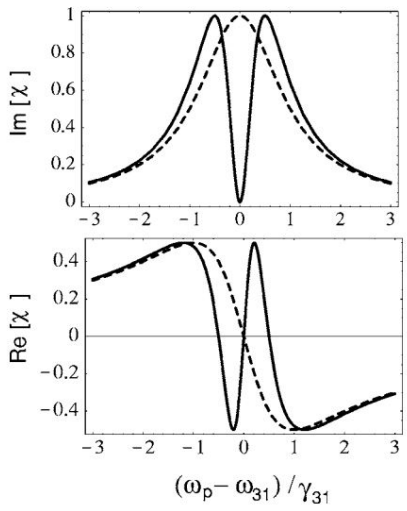

FIGURE 2.2: Real and imaginary parts of linear susceptibility as a function of single-photon detuning $\Delta_1 = \omega_{31} - \omega_p$ in unit of γ_{31} with (solid line) and without(dashed line) the control field coupling

The first term (the real part) of $\chi^{(1)}$ determine the refractive index n while the imaginary part characterize the absorption rate and thus the intensity transmission coefficient $T(\delta)$ for the probe field by the following relations [17, 23]:

$$T(\delta) = \exp\Big\{-Im[\chi^{(1)}]kL/2\Big\} \tag{2.8}$$

$$n(\delta) = 1 + \frac{1}{2}Re[\chi^{(1)}] \tag{2.9}$$

where $k = 2\pi/\lambda$ is the resonant wave number and L is the length of the medium. On two-photon resonance ($\delta = 0$) in the spectrum of $\chi^{(1)}$, the imaginary part of $\chi^{(1)}$ reaches a minimum and vanishes in the approximation of $\gamma_{21} = 0$ for the "dipole-forbidden" transition between state $|1\rangle$ and $|2\rangle$, indicating the zero absorption and the appearance of the transparency window.

2.1.3 Slow light

One essential property of EIT is that the group velocity of light propagating in the atomic medium can be slowed down thus functioning as frozen and stored in the atomic states. The group velocity of probe light is [23, 24]:

$$v_g = \frac{c}{n + \omega_p(dn/d\omega_p)} \approx \frac{\hbar\epsilon_0|\Omega_c|^2}{2\omega_p|d_{13}|^2 N_{atom}} \tag{2.10}$$

where $|\Omega_c|^2 \sim I_c$

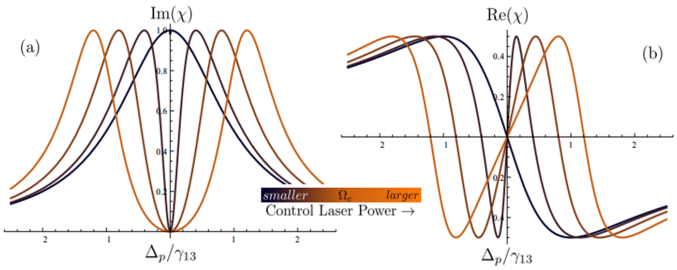

FIGURE 2.3: The evolution of the real and imaginary parts of linear susceptibility as the control field power decreases,indicating the slowing down of the light group velocity

From equation (2.9), the group velocity decreases with control field intensity. This is in fact corresponding to an narrowing width of the absorption (or transmission) spectrum modulated by the factor $(dn/d\omega_p)$ because the curves of real part (dispersion) and the imaginary part (absorption) in Figure 2.2 should have a similar narrow range indicated by Kramers–Kronig relations[25].

As the control field is gradually turned off (adiabatically), the group velocity of the light in the medium reduces to zero. At this time, the photonic state is mapped onto lone-lived states of atoms and retrieved by turning on the control field. Thus, EIT provides a effective tool for the light storage and quantum memory.

2.2 Experimental EIT

2.2.1 ^{87}Rb hyperfine structure

The Rubidium-87 atom can provide the Λ EIT system for its energy structure as shown in Figure 2.4

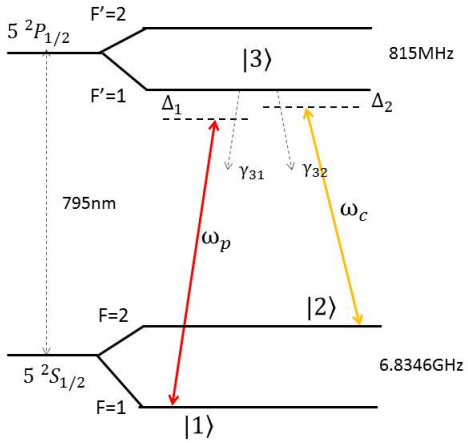

FIGURE 2.4: atomic levels for Λ EIT system. Δ_1 is the single-photon detuning and $\Delta_1 - \Delta_2$ is the two-photon detuning

The probe field frequency is locked to the $5^2S_{1/2}, F = 1 \rightarrow 5^2P_{1/2}, F' = 1$ transition at wavelength of 795 nm and the control field frequency interacts with the $5^2S_{1/2}, F = 2 \rightarrow 5^2P_{1/2}, F' = 1$ transition.

2.2.2 Experimental set-up

The room temperature EIT experiment uses ^{87}Rb vapor cell containing a Ne buffer gas. The cell is first put inside the electromagnetic shield for environment noise filtering and then further shielded by a temperature maintaining cylinder that is connected to a heater and sensors to maintain the cell temperature around $60°$C whch creates the atomic vapor.

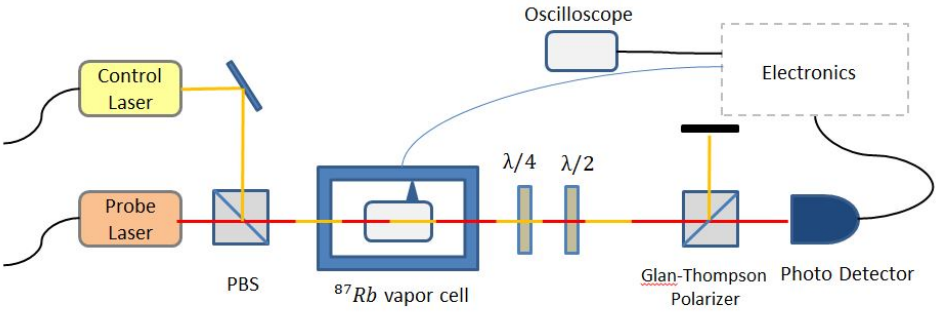

FIGURE 2.5: Schematic experimental EIT set-up. Two beams are co-propagating in the t^{87}Rb cell for EIT

Two diode laser beams, the probe field and control field, are modulated by the laser system composed of two individual acousto-optic modulators (AOM) which shape the probe beams to Gaussian profiles. The two beams are orthogonally polarized to each other so that they can overlap by a Glan-Laser-Polarizer(GLP) and co-propagate through the vapor cell. A half-wavelength plate and a quarter-wavelength plate have to be put after the cell to compensate the effect to the beam polarization by the atom vapors, after which the control field can be filtered out by another GLP or a polarizing beam splitter (PBS), providing the enough attenuation for the probe signal detection.

2.2.3 Data and analysis

In this experiment, the probe field frequency ω_p is locked. Thus the single-detuning Δ is fixed. The control field frequency is scanned from 39.25MHz to 40.75 MHz such that the two-photon detuning $\delta = \omega_{21} - (\omega_p - \omega_c)$ is scanned from -0.75MHz to 0.75MHz to observe the probe transmission of EIT

Raw EIT data

As we can see from Figure2.6, when the control field power is increased, the width of the transparency window is increased as well. The reason for the asymmetry in the above plots is that we were sweeping the two-photon detuning δ rather than the single-photon detuning Δ as the probe field frequency is kept constant. As the control field intensity is zero, the transparency window becomes flat below the transmission power without the memory, which indicates that without the control field coupling, some of the probe light is absorbed by atoms while the other is transmitted.

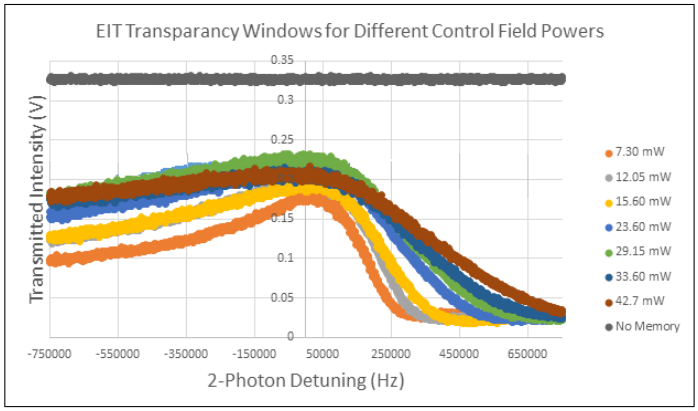

FIGURE 2.6: EIT of ^87Rb vapor cell: transmission power as a function of two-photon detuning for different control field power

EIT window width

The full width at half maximum (FWHM) of the EIT window at different control field power is plotted in Figure2.7. The decreasing of the FWHM indicates the slowing down of the probe light group velocity with the control field power.

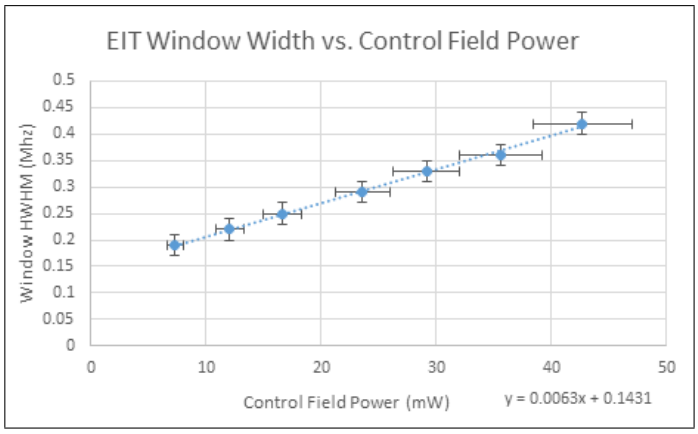

FIGURE 2.7: The FWHM of EIT transparency window appears to increase linearly in size with increasing control field power. The error on power measurements was $\pm 10\%$, and the error on frequency was about ± 0.02 MHz.

EIT data vs. theoretical model

The EIT data of 7.3 mW control field power is plotted with the theoretical model for the intensity transmission coefficient in Figure 2.8 according to equation (2.7), which includes the imaginary part of the susceptibility for the three-level atomic system.

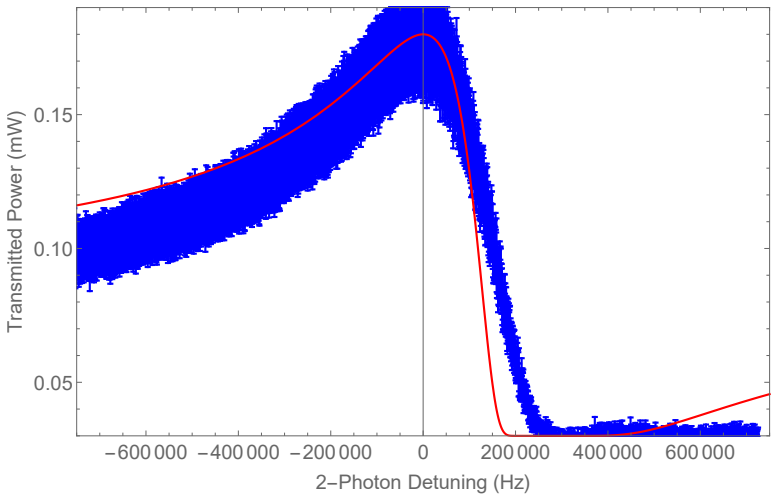

FIGURE 2.8: Fitting of EIT data (blue) to theoretical model (red) for a constant control field power of 7.3 mW. The y-axis is in arbitrary units of power, and the error in power values is $\pm 10\%$. .

The data is in good agreement with the simulation within the 10% uncertainty in transmission measurements, however, we can see that there

is some discrepancy between the width of the experimental data and theoretical model near about +0.2 MHz detuning. The discrepancy may be caused by inhomogeneous broadening of the absorption linewidth due to the Doppler effect[23]. Since we do not take this Doppler broadening into account in our model the transparancy windoww in our data appears wider than in our theoretical model.

Chapter 3

Storage of light

The storage of light is a key for the memory of quantum light and thus for long distance quantum communication. After the light group velocity of light was reduced to 17m/s using EIT for ultracold atoms [24], the storage and retrieval of a classical light has been realized using cold atoms[26] as well as warm Rb vapor[27]. Due to the decoherence and excitation decay, however, the storage time is always limited. There exists a trade-off between the storage time and efficiency for both classical and quantum light. In this chapter, we test the the storage of classical light based on the room temperature EIT system introduced in Chapter 2.

3.1 Propagation theory

The propagation of the probe light in an EIT medium is described by the Heisenberg equation[17] :

$$(\frac{\partial}{\partial t} + c\frac{\partial}{\partial z})\hat{E}(z,t) = igN\hat{e}(z,t) \tag{3.1}$$

$$\hat{e}(z,t) = -\frac{i}{\Omega_c}[\frac{\partial}{\partial t}\hat{s}(z,t)] \tag{3.2}$$

$$\hat{s}(z,t) = -\frac{g\hat{E}(z,t)}{\Omega_c} \tag{3.3}$$

where $\hat{E}(z,t)$ is the electric field strength $g^2 = \frac{|d_{13}|^2}{\epsilon_0 \hbar V}$is the atom-field coupling constant, $\hat{e}(z,t)$ describe the atomic polarization and $\hat{s}(z,t)$ describes the spin wave. The solution of the equations can be obtained by introducing a quantum field $\Psi(z,t)$ which is the superposition of the electric wave and spin wave:

$$\Psi(\hat{z},t) = \cos\vartheta\hat{E}(z,t) - \sin\vartheta\sqrt{N}\hat{s}(z,t) \tag{3.4}$$

Here $\cos\vartheta = \frac{\Omega_c}{\sqrt{\Omega_c^2+g^2N}}$, $\sin\vartheta = \frac{\Omega_c^2+g^2N}{\sqrt{\Omega_c^2+g^2N}}$. The quantum field is ruled by the equation

$$(\frac{\partial}{\partial t} + c\cos\vartheta^2\frac{\partial}{\partial z})\hat{\Psi}(z,t) = 0 \tag{3.5}$$

This is a equation of propagation with group velocity $v_g = c\cos\vartheta^2$ with preserved shape. As the control field power (Rabi frequency) decreases to zero, the light pulse is frozen, and can be reaccelerated with preserved classical properties after the control field is turned on. The propagation

process can be numerically simulated and Figure 3.1 shows some example results done by M. D. Lukin[17]

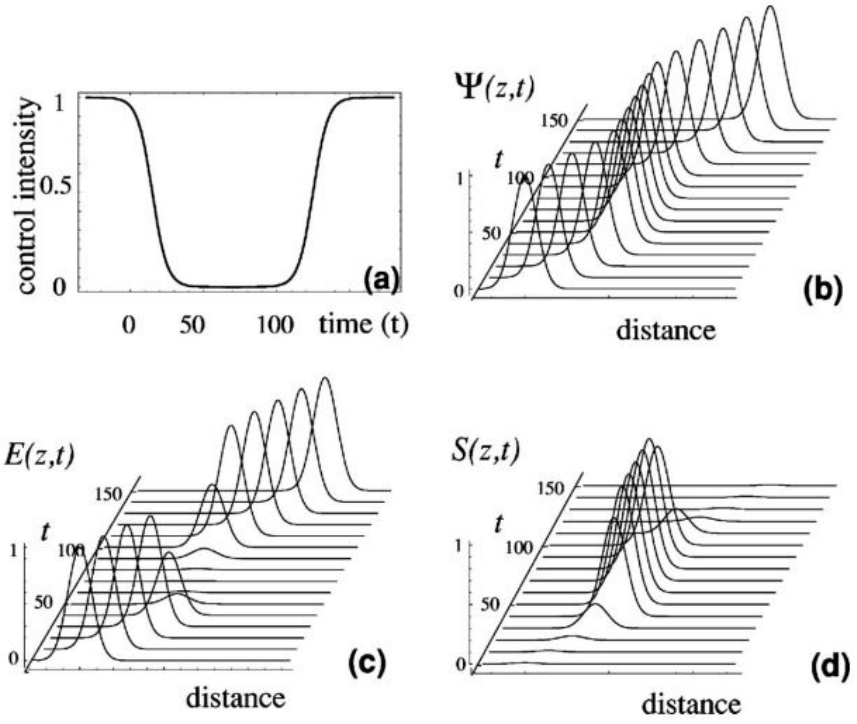

FIGURE 3.1: Simulated evolution of dark state propagation: (a) control field power and the amplitude, (b) quantum field Ψ, (c) electric field, and (d) spin

3.2 Experimental methods

3.2.1 EIT set-up

The experimental set-up for the room temperature storage of light is based on the EIT experimental set up as discussed in Chapter 2. As shown in Figure 2.5, the probe and control field are co-propagating through the Rubidium vapor cell. The AOM system can also control the read-write sequence of the control field to store and retrieve the probe light. A filter system (Fabry-Perot etalons) is also required for detecting the transmitted light. Details are introduced in Chapter 4.

Rather than scanning the control field frequency to measure the EIT feature, here we phase-lock the control field to the probe field to construct a phase-coherent laser system.

3.2.2 Phase lock

The group velocity of probe light is slowed down at the EIT transparency window when the two-photon detuning is zero, meaning the frequency difference of control laser and probe laser is 6.8346 GHz, according to the energy structure of ^{87}Rb shown in Figure 2.4. The phase-coherence of the probe and control beams is crucial for the successful storage of light. A

phase-lock system, which uses a feedback optical phase-locked loop (OPLL) is described in Figure 3.2

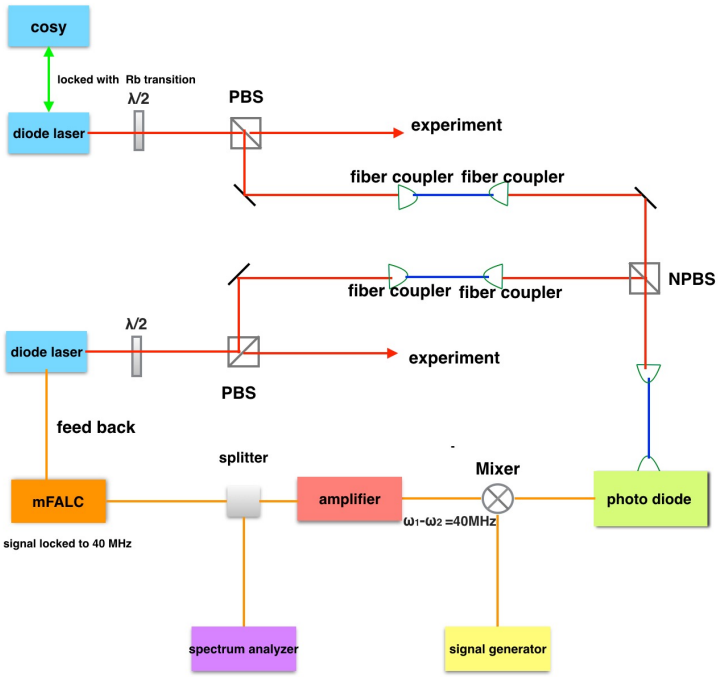

FIGURE 3.2: Phase-lock system: The probe and control laser are overlapped and interfere to generate a beat note with frequency corresponding to their frequency difference. The beat note is mixed to low frequency as the feed back of the PID control.

The interference of probe and control field causes a "beat note" with frequency equal to their relative frequency $\omega_p - \omega_c$, which is around 6.8346 GHz. This relative frequency is drifting and fluctuating in reality, thus we need phase lock to make it stable. The beat note is first mixed with a 6.8775 GHz signal from the generator, modulated to around 40 MHz so that it can be detected. The resulting signal is sent to the PID controller as the feed back for shaping the input laser.

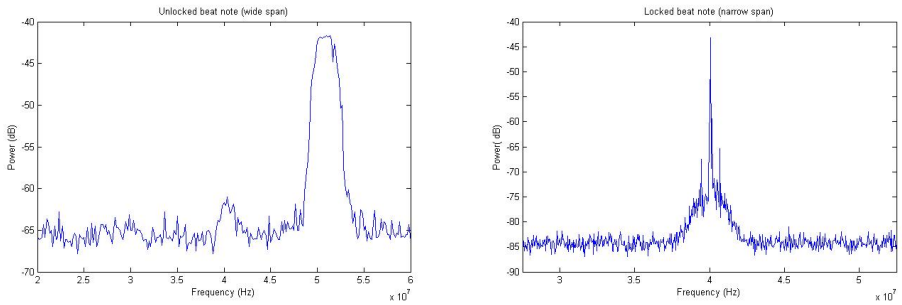

(A) (B)

FIGURE 3.3: Power of modulated beat note signal (A) before and (B) after the phase lock.

As a result, 87% of the modulated beat note power is locked around 40 MHz, meaning most of the original relative frequency of probe and control

field is locked around 6.8346 GHz. The modulated probe and control field beat note signal before and after phase-lcok is shown in Figure 3.3

3.3 Results and analysis

The input probe signals for both situation: with and without atomic vapor cell are first detected. After that, the probe signal under the EIT operation is detected as the storage signal. The data is collected through electronic-controlled repeating operation, where the control field is set to turn off for about 1 μs as the storage time on each repeating sequence. The probe signal data is shown as pulses in Figure 3.4a and as a comparison with simulated results in Figure 3.4b.

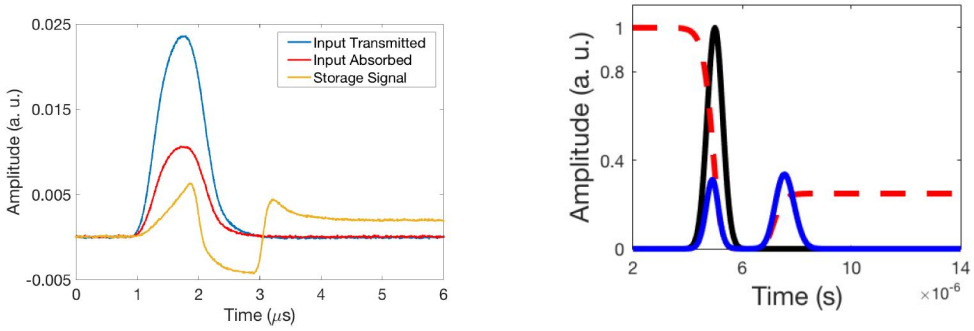

(A) (B)

FIGURE 3.4: Storage of light and readout: (A) data plotted: input pulse without (blue) and with (red) the absorption of atomic vapor cell. The storage signal (yellow) are split by two parts, the front indicates the leakage while the behind part is the retrieved signal after storage (B) simulation of experiment including input (black), control field (red dashed) and storage (blue) amplitudes.

According to Figure 3.4a, the storage time of the probe signal is around 1 μs when the control field is off. The storage signal between $1\ \mu s < t < 2\ \mu s$ is the leakage that is not converted to atomic state and stored. The higher flat tail indicates the noise from the control field.

As the properties of the classical light are preserved after storage, we mainly concentrate on the efficiency of the storage η. This is calculated as the fraction of the input power that is retrieved after being transmitted through the filtering but without being absorbed by the atomic vapor. Thus η can be calculated by integrating the retrieved probe signal over the region of interest (ROI) around 3 μs to 4 μs comparing to the integration of the input (blue) from 1 μs to 2.5 μs. By controlling the reading and writing sequences of control field, we can manipulate the storage time and test the corresponding storage efficiency. An exponential decay of the efficiency is observed as shown in figure 3.5.

The data follows the exponential decay $\eta \propto e^{-\Gamma t}$ where Γ is the decoherence rate and t is the storage time. By fitting the data, Γ, is estimated to be 1 MHz, indicating the coherence time of the Rubidium atoms is $\alpha = 1/\Gamma = 1\ \mu s$.

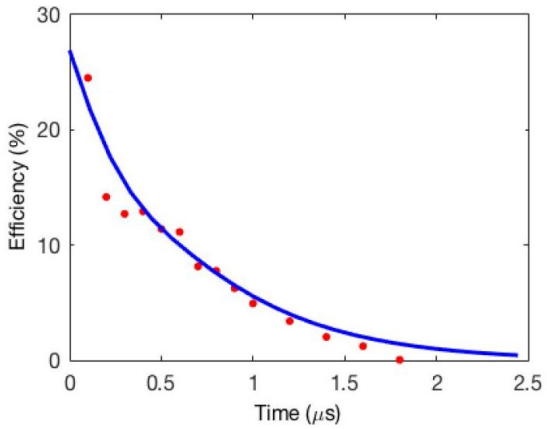

FIGURE 3.5: Storage efficiency vs storage time. The plots are fit with an exponential curve from simulation.

The effects such as the atomic radiative decay, thermal collision, Doppler shift and the incomplete light-matter interaction possibly contributed to the decoherence of the atoms. Besides, the write-read of the control field is not a perfect adiabatic process, which influences coherence time as well.

Some efforts could be proposed to improve the storage efficiency, which becomes more important when moving towards the storage of light at single-photon level. For example, coating the inner cell wall with paraffin layer for lowering the temperature to reduce the thermal motion[28]. Also, a cavity system could be applied to strengthen the light-matter interaction, which will be discussed in Chapter 5.

Chapter 4

Portable quantum memory

The room temperature quantum memory with vapor cell benefits from its space-saving and easy operation without the need for laser cooling and trapping. This makes it possible for building portable quantum memory nodes. This also provides a flexible platform for scalable quantum information processing such as long distance quantum communication.

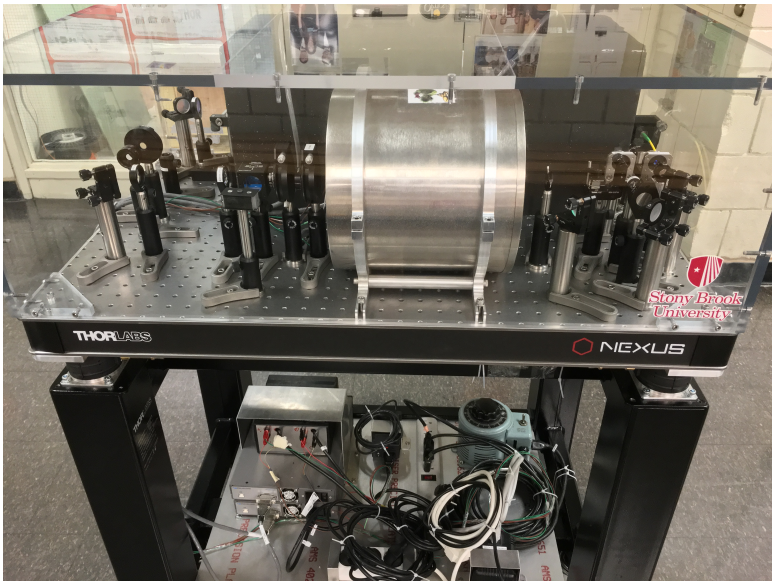

FIGURE 4.1: Built portable quantum memory system

4.1 Description of set-up

4.1.1 Portable optical table

The portable quantum memory platform is based on a $25'' \times 35''$ optical table from ThorLab, which is held on a framework with detachable casters as the pictures shows in Figure 4.1. The electronics, including the temperature controllers and a variac, are fixed on a layer under the optical table to make up the whole memory system

4.1.2 Temperature control system

The ^{87}Rb cell needs to be maintained at around 60°C to keep the atoms in a stable vapor state. The temperature control system consists of two

parts: one heater for heating the inner shield and one temperature sensor connected to the cell. The feedback system maintain the cell temperature around 60°C with the fluctuation within 0.1 °C at equilibrium. The construction of this temperature system also includes wire connecting and soldering. The controller and display panel of the electronics meters are shown in Figure 4.2.

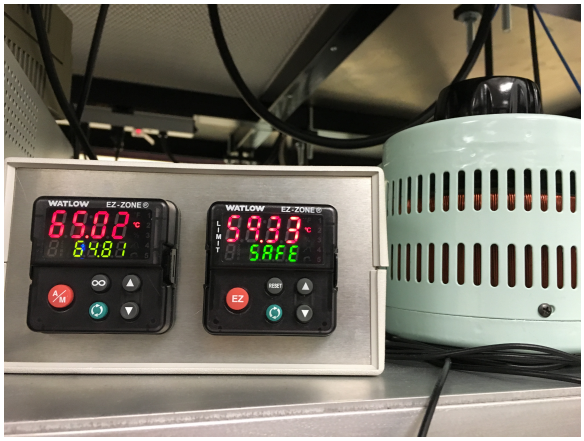

FIGURE 4.2: Temperature control box: the left sensor is connected to the heater while the right detects the cell's temperature. The two controllers are part of a feed-back electronics system to maintain the cell temperature around 60°C at equilibrium.

4.1.3 Filtering system

The room temperature quantum memory is constrained by because of the low signal-to-noise-ratio, thus requires a fine filtering system to minimize the noise while optimizing the probe signal. Accordingly,a single photon is accompanied by 10^{12} background photons, meaning 120dB background-to-signal ratio[21].

The main noise comes from the control field that co-propagates with the probe field. A polarizing beam spliter (PBS) can filter the control fields by 42dB attenuation and keep 80% transmission of probe field. Two etalons can together provide 102dB filtering of control field with about 10% total probe transmission. A Faraday isolator with 50% transmission is put between two etalons to reject the reflection of etalon surfaces. The overall system provide 140dB control field suppression while 10dB probe attenuation, which achieves 130dB control/probe suppression ration aiming to compensate the 120dB background-to-signal ratio.

Fabry-Perot Etalons

Because of the interference of the multiple reflections of beams between two reflecting surfaces, the total transmission of an etalon varies with the optical path length of the beam through it. Suppose an etalon consists of two identical surfaces with reflectance R and transmission T and material with refractive index n between them, as shown in Figure 4.3.

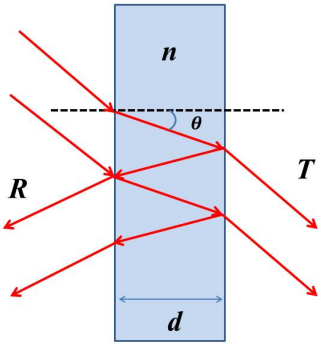

FIGURE 4.3: A Fabry–Pérot etalon. A beam enters the etalon and undergoes interference due to multiple internal reflections.

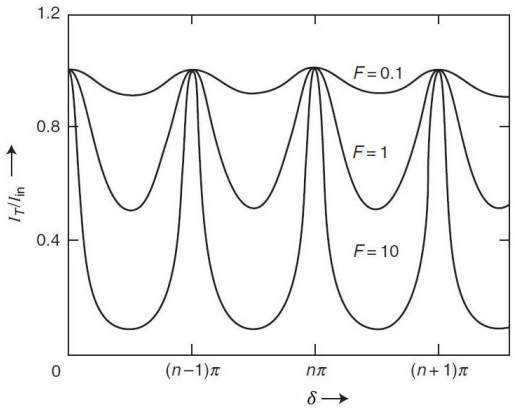

FIGURE 4.4: The transmission of a Fabry–Pérot etalon as function of δ for different F values.

After each internal reflection, the beam gains a phase difference of

$$\delta = \frac{2\pi}{\lambda} 2nd\cos\theta \tag{4.1}$$

The transmitted fraction of the input light is

$$I_T/I_0 = \frac{T^2}{(1-R)^2}\frac{1}{1+F\sin^2\frac{\delta}{2}} \tag{4.2}$$

where

$$F = \frac{4R}{(1-R)^2} \tag{4.3}$$

The resonance frequency spacing as shown in Figure 4.4 is called *free*

spectral range. The ratio of free spectral range ν_{FSR} and width of the frequency band or ν_{FWHM} can be derived to be

$$\mathcal{F} = \frac{\nu_{FSR}}{\nu_{FWHM}} = \frac{\pi}{2}\sqrt{F} \approx \frac{\pi\sqrt{R}}{1-R} \tag{4.4}$$

This is called *finesse*, which is an important parameter of a Fabry–Pérot etalon. For an etalon with two different surface, we can correct the equation 4.4 with $R = \sqrt{R_1 R_2}$ and get

$$\mathcal{F} \approx \frac{\pi \sqrt[4]{R_1 R_2}}{1-\sqrt{R_1 R_2}} \tag{4.5}$$

In this setup, we used two etalons whose size is linearly controlled by temperature with the coefficient of linear expansion around $8.6 \times 10^{-6}/K$. The temperature stability is 0.01K. The etlon finesse is 310 with corresponding FWHM of 40MHz for 795nm probe laser.

Gaussian mode

The input beam is shaped as Gaussian beam, whose power is concentrated in around the beam center. Because of the boundary conditions of the etalon, the beam has different transverse electromagnetic modes (TEM) which are the solutions of the Maxwell equations.

The intensity pattern of TEM, also referred to as Hermite-Gaussian (HG) modes, is represented by Hermite polynomials:

$$I_{mn}(x,y) = I_0[H_m(\frac{\sqrt{x}}{w})\exp\left(\frac{-x^2}{w^2}\right)]^2[H_n(\frac{\sqrt{y}}{w})\exp\left(\frac{-y^2}{w^2}\right)]^2 \tag{4.6}$$

The lowest order is when $m = n = 0$ with corresponding TEM_{00} mode:

$$I(r,z) = I_0(\frac{w_0}{w})^2\exp\left(\frac{-2r^2}{w^2}\right) \tag{4.7}$$

which is the Gaussian mode.

For boundary conditions with cylindrical symmetry, the transverse modes are Gaussian characterized by Laguerre polynomials. Representing intensity in polar coordinates, the transverse modes are:

$$I_{pl}(\rho,\phi) = I_0\rho^l[L_p^l(\rho)]^2\cos^2(l\phi)e^{-\rho} \tag{4.8}$$

where $\rho = 2r^2/w^2$ and L_p^l is the Laguerre polynomial. For $p = l = 0$, the TEM_{00} mode also reduces to a Gaussian.

The intensity patterns of equation 4.6 and equation 4.8 are shown in Figure 4.5

4.1.4 Optics alignment

The filtering setup requires a very precise alignment of etalons. Two etalons are mounted into the custom machined cubes that are fixed to temperature controllers. Thermal paste is applied on the etalon-cube interfaces and cube-controller interfaces to make sure the good thermal conduct. By

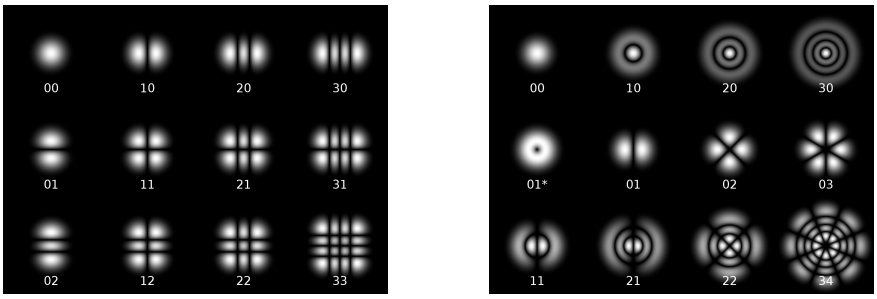

(A) Rectangular TEM (mn) (B) Cylindrical TEM (pl)

FIGURE 4.5: TEM modes of etalon

slightly changing the etalon temperature, the refractive index changes to optimize the transmission of the probe beam through both etalons.

We used two etalons to accomplish the aforementioned filtering but due to unavoidable reflections, the beam transmitted through the first etalon might interference with the beam reflected by the second. To avoid this unintended consequence, a Faraday isolator is put between the etalons to reject the reverse beam and allow the beams to pass in only one direction.

Each etalon also requires two lenses with focal length of 200mm to form a con-focal alignment to focus the beam onto the flat surface of etalon and then collimate afterwards. The set up of the filtering system is shown in Figure 4.6a. The two etalons are fixed on a custom machined base that keeps them in the same height and in straight line. One of them can have longitude transition such that it can be aligned without walking the mirror again when the first etalon is aligned.

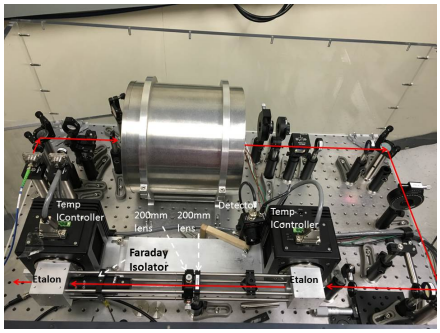

(A) Filtering system

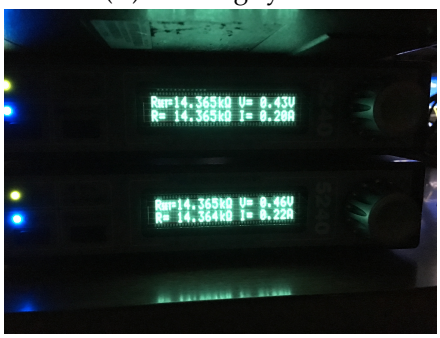

(B) Temperature controller of etalons

FIGURE 4.6: Etalon setup

The TEM_{00} mode of the beam transmitted through both etalons is desired. To achieve this, the beam should perpendicularly hit the center of each etalon. We use a profiler to detect the beam image and align the etalons sequentially.

To align the first etalon, we first horizontally and vertically walk the mirror and adjust the lens position to optimize the position that the beam hits the etalon. We can then compensate the deflection and eliminate the higher order rectangular TEM mode to get a concentric image. The TEM_{00} mode can then be obtained by tuning the etalon temperature smoothly through the controller shown in Figure 4.6b. The second etalon is aligned in a similar way by adjusting the lens position and tuning the etalon temperature to get a Gaussian beam image. A image of the TEM_{00} mode of the successfully aligned etalon is shown in Figure 4.7.

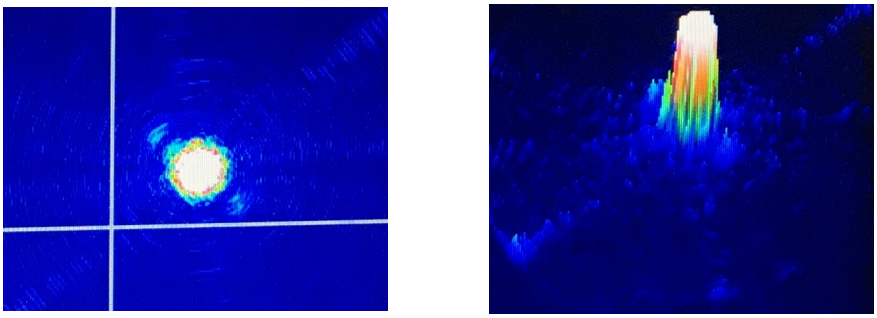

(A) 2D plot image (B) 3D plot image

FIGURE 4.7: The images of the (Gaussian) mode transmitting the etalon plotted by the profiler.

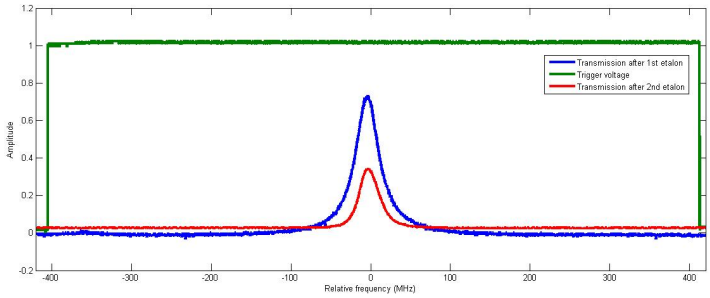

FIGURE 4.8: Transmission of Etalons: two etalons are optimized to have the transmission peaks on the $5^2S_{1/2}, F = 1 \rightarrow 5^2P_{1/2}, F' = 1$ transition frequency of ^{87}Rb at the same time.

To get the maximum transmitted power, and consequently efficiency, we used the detector and oscilloscope to optimize the transmission signal by wither tuning the etalon temperature or slightly adjusting the optics. The maximum transmission occurs only when the transmission peaks of two etalons occurs at the same frequency, which corresponds the probe field frequency that should be locked to the $5^2S_{1/2}, F = 1 \rightarrow 5^2P_{1/2}, F' = 1$ transition of ^{87}Rb. A trigger voltage is used to scan the probe laser frequency, which is centered right on the $5^2S_{1/2}, F = 1 \rightarrow 5^2P_{1/2}, F' = 1$ transition frequency and within a range of 816MHz. The transmission signal of both

etalons is shown in Figure 4.8.By measuring the power of the probe laser before and after the etalons at the locked frequency, we get about 30% transmission of each etalon and 5% transmission for the whole filtering system, which is good enough for the experiment operation.

4.2 Storage of light at single-photon level

We tested the portable quantum memory system by the storage of light experiment at the single-photon level. The set-up is shown in Figure 4.9. The probe pulse is detected by a single-photon counter and the input pulse is manipulated to one single photon per pulse on average. The input signal after the absorption of atomic cell and the storage signal is shown as histogram in Figure4.10

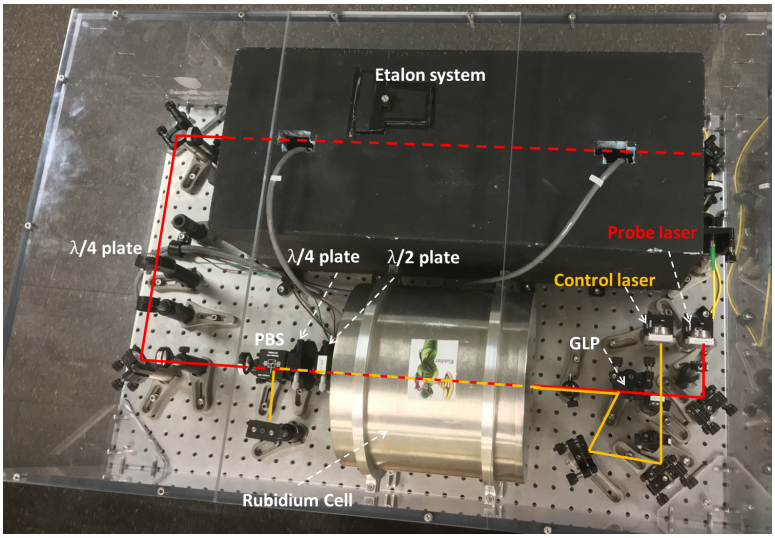

FIGURE 4.9: Optics alignment of portable quantum memory. The single-photon level storage of light was operated on this platform. The back box is for maintaining stable temperature of etalons

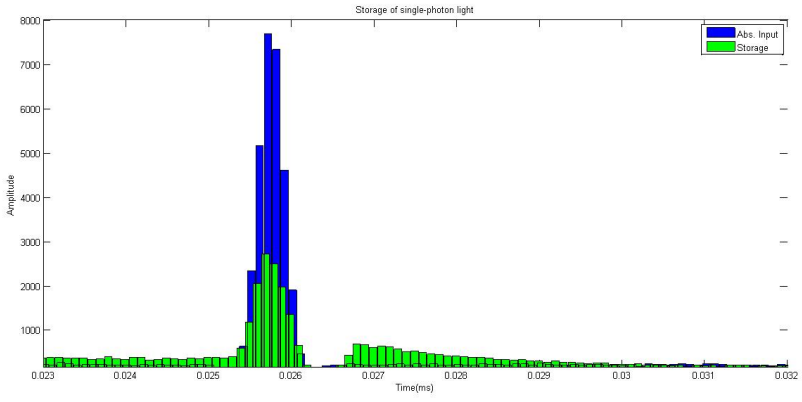

FIGURE 4.10: Storage of single-photon light. The blue histograms are the input probe pulse transmitting the atom cell while the green histograms are the storage signal

According to the green histogram, the storage time is $1\ \mu s$from 25 μs to 26 μs. We integrated the retrieved pulse signal and the background signal over the corresponding region of interest(ROI) to estimate that the efficiency. The ROI1 for the retrieved signal from $26.7\ \mu s$ to $29.7\ \mu s$ has the counting rate of 0.5035% photon/pulse and The ROI2 for background signal from $32\ \mu s$ to $35\ \mu s$ has has the counting rate of 0.2476% photon/pulse, indicating the net retrieved signal has around $0,25\%$ photons/pulse. Considering the input probe signal contains a single-photon per pulse and only 5% is transmitted to the filtering system, the storage efficiency is estimated to be 5%. The efficiency of storage could be possibly improved by adopting cavities to the EIT system to strengthen the light-matter coupling.

Even we have applied the filtering system that could ideally suppress 130dB noise from the control field which surpasses the required the filtering of 120dB noise, there is still unexpected noise such as spontaneous Raman scattering. After we subtracted the noise from both ROI1 and ROI2, we got a signal-to-background ratio of 4.2, which is good enough for achieving the single-photon storage of polarization states with high fidelity[21].

Chapter 5

Outlook

5.1 EIT with cavities

A way to improve the efficiency of the storage is to strengthen the coupling of light and atomic vapor. One possible approach is applying a Fabry-Perot cavity where the light is reflected and interacts with atomic vapor multiple times before it transmits through the cavity. A confocal cavity structure can be constructed by two mirrors with radius of curvature of 20mm and separated by about 40mm to each other as shown in Figure 5.1

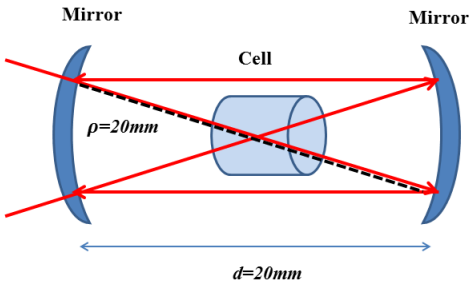

FIGURE 5.1: Confocal cavity

The total transmission of the Fabry-Perot cavity can be calculated by the reflectance of the two mirror according to the discussion in section 4.1.3. For cavities with two different mirrors, the total transmission is

$$I_T/I_0 = \frac{T_1 T_2}{(1-\sqrt{R_1 R_2})^2} \frac{1}{1+F\sin^2\frac{\delta}{2}} \tag{5.1}$$

The parameters of the cavity can be engineered by using different mirror combinations according to the desire for cavity. Some calculation are listed in Table 5.1

TABLE 5.1: Calculated parameter of the confocal cavity with mirror of different reflectance

R_1	R_2	Total Transmission	finesse	ν_{FWHM}(MHz)
0.99	0.99	1	312	24
0.99	0.9999	0.039	619	12
0.99	0.98	0.887	208	36
0.98	0.9999	0.020	309	24

5.2 Storage of polarized qubits

To realize the storage of a qubit, we need to encode the polarization to a qubit to form a superposition quantum state:

$$|\Psi\rangle = \cos\theta\,|H\rangle + e^{i\phi}\sin\theta\,|V\rangle \tag{5.2}$$

As a single photon with superposition state of polarization enters beam displacer, its pathway is undetermined as following the principle of quantum mechanics. By putting a memory system on both pathway, we intend to map the superposition state to the collective atomic state and retrieve the state at a later time. The basic set-up of the qubit storage is shown in Figure 5.2

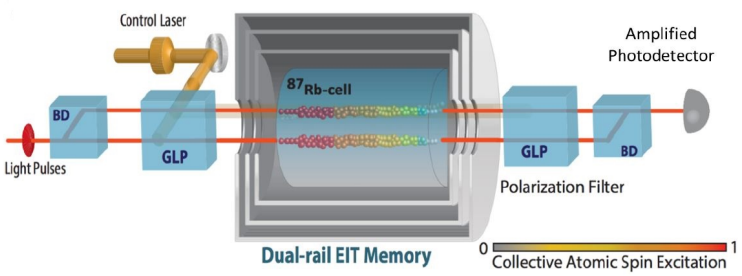

FIGURE 5.2: Storage of qubit set-up

We plan to combine cavities with the dual EIT system to promote the performance of room temperature storage of qubits. Two cavities are needed on both pathways that pass through the atomic vapor cell. Since the atom cell aperture has a diameter of 4 mm, we need the two parallel cavities to be close enough to each other. Thus, we need the clear-edge mirrors to hold the mirror with about 4 mm diameter. Also, a custom machined adapter is needed to mount the mirror to the 1/2" mirror mount.

The mirror mounts should be fixed and on a base in the cylindrical shield such that the the cavities are beside the center axis of the shield. The schematic is shown in Figure 5.3a.

An important consideration is the thermal stability of the cavities when heating base. To minimize the thermal effect that may deform the cavity, the metal with low coefficient of thermal expansion (CTE) such as Invar is considered to cut as the cavity base. Besides, a screwable mirror holder and a piezo can be applied to each mirror of a cavity to adjust the cavity length either mechanically or electronically to from a re-entrant that is able to be

locked to the laser frequency with thermal stability. The schematic of this design is shown in 5.3c.

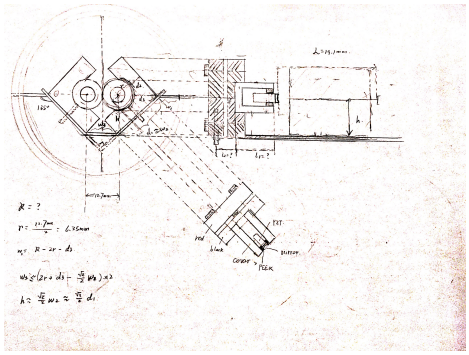

(A)

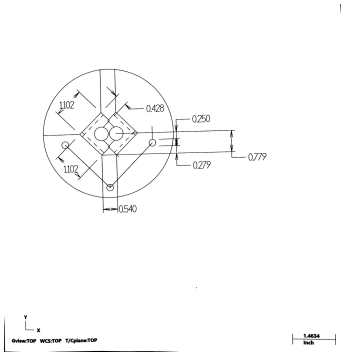

(B)

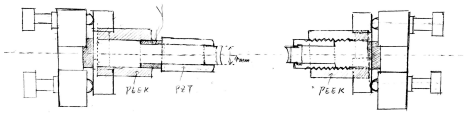

(C)

FIGURE 5.3: Schematics of the dual-cavity design

Bibliography

1. Schaller, R. R. Moore's law: past, present and future. *IEEE spectrum* **34,** 52–59 (1997).
2. Feynman, R. P. There's plenty of room at the bottom. *Engineering and science* **23,** 22–36 (1960).
3. Monroe, C. Quantum information processing with atoms and photons. *Nature* **416,** 238–246 (2002).
4. Knill, E., Laflamme, R. & Milburn, G. J. A scheme for efficient quantum computation with linear optics. *nature* **409,** 46–52 (2001).
5. Shor, P. W. Polynomial-time algorithms for prime factorization and discrete logarithms on a quantum computer. *SIAM review* **41,** 303–332 (1999).
6. Einstein, A., Podolsky, B. & Rosen, N. Can quantum-mechanical description of physical reality be considered complete? *Physical review* **47,** 777 (1935).
7. Bennett, C. H. *et al.* Teleporting an unknown quantum state via dual classical and Einstein-Podolsky-Rosen channels. *Physical review letters* **70,** 1895 (1993).
8. Bouwmeester, D. *et al.* Experimental quantum teleportation. *Nature* **390,** 575–579 (1997).
9. Bennett, C. H. & Brassard, G. Quantum cryptography: Public key distribution and coin tossing. *Theoretical computer science* **560,** 7–11 (2014).
10. Cirac, J. I. & Zoller, P. Quantum computations with cold trapped ions. *Physical review letters* **74,** 4091 (1995).
11. Steane, A. The ion trap quantum information processor. *Applied Physics B: Lasers and Optics* **64,** 623–643 (1997).
12. Wootters, W. & Zurek, W. Nature 299 802 Dieks D 1982. *Phys. Lett. A* **92,** 271 (1982).
13. Sangouard, N., Simon, C., De Riedmatten, H. & Gisin, N. Quantum repeaters based on atomic ensembles and linear optics. *Reviews of Modern Physics* **83,** 33 (2011).
14. Briegel, H.-J., Dür, W., Cirac, J. I. & Zoller, P. Quantum repeaters: the role of imperfect local operations in quantum communication. *Physical Review Letters* **81,** 5932 (1998).
15. Zukowski, M, Zeilinger, A, Horne, M. & Ekert, A. " Event-ready-detectors" Bell experiment via entanglement swapping. *Physical Review Letters* **71,** 4287–4290 (1993).
16. Afzelius, M. *et al.* Photon-echo quantum memory in solid state systems. *Laser & Photonics Reviews* **4,** 244–267 (2010).

17. Lukin, M. Colloquium: Trapping and manipulating photon states in atomic ensembles. *Reviews of Modern Physics* **75,** 457 (2003).

18. Cirac, J. I., Zoller, P., Kimble, H. J. & Mabuchi, H. Quantum state transfer and entanglement distribution among distant nodes in a quantum network. *Physical Review Letters* **78,** 3221 (1997).

19. Abdumalikov Jr, A. *et al.* Electromagnetically induced transparency on a single artificial atom. *Physical review letters* **104,** 193601 (2010).

20. Novikova, I., Walsworth, R. L. & Xiao, Y. Electromagnetically induced transparency-based slow and stored light in warm atoms. *Laser & Photonics Reviews* **6,** 333–353 (2012).

21. Kupchak, C. *et al.* Room-temperature single-photon level memory for polarization states. *Scientific reports* **5** (2015).

22. Harris, S. E. *Electromagnetically induced transparency* in *Quantum Electronics and Laser Science Conference, 1997. QELS'97., Summaries of Papers Presented at the* (1997), 25–25.

23. Fleischhauer, M., Imamoglu, A. & Marangos, J. P. Electromagnetically induced transparency: Optics in coherent media. *Reviews of modern physics* **77,** 633 (2005).

24. Hau, L. V., Harris, S. E., Dutton, Z. & Behroozi, C. H. Light speed reduction to 17 metres per second in an ultracold atomic gas. *Nature* **397,** 594–598 (1999).

25. Grundmann, M. in *The Physics of Semiconductors* 775–776 (Springer, 2010).

26. Liu, C., Dutton, Z., Behroozi, C. H. & Hau, L. V. Observation of coherent optical information storage in an atomic medium using halted light pulses. *Nature* **409,** 490–493 (2001).

27. Phillips, D., Fleischhauer, A, Mair, A, Walsworth, R. & Lukin, M. D. Storage of light in atomic vapor. *Physical Review Letters* **86,** 783 (2001).

28. Balabas, M., Karaulanov, T., Ledbetter, M. & Budker, D. Polarized alkali-metal vapor with minute-long transverse spin-relaxation time. *Physical review letters* **105,** 070801 (2010).